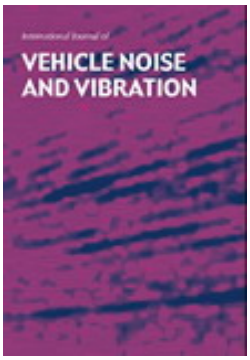


**International Journal of Vehicle Noise and Vibration**

ISSN online: 1479-148X - ISSN print: 1479-1471
https://www.inderscience.com/ijvnv

# Investigation of liner and duct geometry discontinuities on the attenuation of resonator Helmholtz lined duct element

Raja Dhief, Mohamed Taktak, Mabrouk Chaabane, Mohamed Haddar

**DOI:** 10.1504/IJVNV.2022.10050580

**Article History:**
Received: 19 April 2021
Accepted: 13 September 2021
Published online: 16 September 2022

# Investigation of liner and duct geometry discontinuities on the attenuation of resonator Helmholtz lined duct element

Raja Dhief and Mohamed Taktak*

Laboratory of Mechanics, Modeling and Production,
Mechanical Engineering Department,
National School of Engineers of Sfax,
BP 1173 – 3038, Sfax, Tunisia
and
Faculty of Sciences of Sfax,
University of Sfax,
Sfax, Tunisia
Email: dhief.raja@yahoo.fr
Email: mohamed.taktak@fss.rnu.tn
*Corresponding author

Mabrouk Chaabane

Faculty of Sciences of Sfax,
University of Sfax,
Sfax, Tunisia
Email: mabrouk.chaabane@fss.usf.tn

Mohamed Haddar

Laboratory of Mechanics, Modeling and Production,
Mechanical Engineering Department,
National School of Engineers of Sfax,
BP 1173 – 3038, Sfax, Tunisia
Email: mohamed.haddar@enis.rnu.tn

**Abstract:** In this study, the acoustic performance of the liner characteristics coupled with geometric discontinuities on the acoustic attenuation of a lined duct is investigated. The model is based on the computation of the scattering matrix. The liner is composed of a perforated plate with an air cavity backed by a rigid wall plate. The parametric study was conducted for six configurations, including cases of sudden or progressive narrowing and widening of the duct radius. The numerical results show the relative influence of the variation of each parameter, and of each type of radius discontinuities of ducts on the acoustic power attenuation.

**Keywords:** acoustic lining; cylindrical duct; discontinuity effect; acoustic attenuation.

**Reference** to this paper should be made as follows: Dhief, R., Taktak, M., Chaabane, M. and Haddar, M. (2022) 'Investigation of liner and duct geometry discontinuities on the attenuation of resonator Helmholtz lined duct element', *Int. J. Vehicle Noise and Vibration*, Vol. 18, Nos. 1/2, pp.77–101.

**Biographical notes:** Raja Dhief is a PhD Doctor in Physics. She received her Doctorate in Physics from the Faculty of Sciences of Sfax (FSS), Sfax, Tunisia in 2021. The subject of her PhD thesis is related to the numerical characterisation of the acoustic propagation in ducts with geometry and impedance discontinuities.

Mohamed Taktak graduated from the National School of Engineers of Sfax, Tunisia. He holds a PhD in 2008 in the field of Mechanical Engineering from ENIS, Tunisia and the University of Technology of Compiègne, France. His research areas of interest are the vibro-acoustic modelling and diagnostics of structures and mechanical systems also numerical and experimental methods in vibroacoustics. He published several papers in refereed journals.

Mabrouk Chaabane is a Professor in Physics in the Faculty of Sciences of Sfax. His research areas of interest are the physics of the environment and the climate as well as the study of acoustic problems like the acoustic propagation in duct systems and in porous materials. He published several papers in refereed journals in these topics.

Mohamed Haddar is a Professor at the National School of Engineers of Sfax in Tunisia, his main research interests are the dynamic and modelling of structures, mechanical systems, vibro-acoustics and fluid structure interaction. He published over 120 papers in international journals. He is the Director of 60 theses. He was a chair of five national and international congresses and referee for national and international journals.

## 1 Introduction

Sound propagation in ducts systems is a problem of considerable practical interest for aero-engines. One of the problems treated in this field is the development of acoustic liners to reduce noise in these systems. The Helmholtz resonator is one of these acoustic liners. The absorbing mechanism of this liner is simple: the wave is propagated across the perforations and a part of the acoustic energy is dissipated by friction and heat exchanges with liner layers. The acoustic performance of Helmholtz resonator lined duct has been studied in several works as presented in Homentcovschi and Miles (2010), Xu and Cheuk-Ming (2012), Ni et al. (2017), Martin and Michael (2018) and Knobloch et al. (2018). The disadvantage of this liner consists in a narrow attenuation peak. Other concepts can provide broader noise attenuation band such as duct discontinuities that ameliorate the reflection of the sound wave. The acoustic behaviour of ducts with section changes has been treated by means of some matrices, such as the transfer matrix as presented in Peat (1988) and Sitel et al. (2006), the reflection matrix by Akoum and Ville (1998), the transmission matrix by Sitel et al. (2003) and the scattering matrix presented by Demir (2016, 2017) and Miles (1946). The multimodal scattering matrix allows, in high mode propagation conditions, the characterisation of geometric and impedance discontinuities because it is an intrinsic propriety of the duct element. Taktak et al. (2010,

2012, 2013) developed a numerical method to compute the multimodal scattering matrix using the finite element method of an axisymmetric lined duct in the cases with and without flow. Then, this method was improved to incorporate the temperature effect (Ben Jedidia et al., 2016). The effect of porous liner characteristics on the acoustic attenuation of lined duct was studied by Othmani et al. (2015) and the geometry effect on the acoustic behaviour of a porous lined duct was studied by Masmoudi et al. (2017) and Dhief et al. (2020).

In this work, an extension of these previous works is presented: the effect of geometry and liner characteristics composed of a perforated plate with an air cavity backed by a hard wall plate on the acoustic power attenuation of various ducts discontinuities configurations is investigated, based on the use of a numerical model to compute the multimodal scattering matrix. Using this matrix, the acoustic power attenuation is computed. In the present paper, six configurations of cylindrical ducts are studied, presenting cases of narrowing and widening of a radius duct with sudden or progressive discontinuities. The paper is structured as follows: in Section 2, the description of the studied problem and the computation of the impedance of locally reacting liner are presented. Section 3 displays the numerical computation of the multimodal scattering matrix. Section 4 evinces the acoustic power attenuation computation. Finally, numerical results are presented and discussed in Section 5, which aims to evaluate the influence of geometry and liner characteristics on the acoustic power attenuation of each studied configuration.

## 2 Description of geometries of studied ducts and normalised acoustic impedance of the liner

The studied ducts are 1 m length ducts. They present a section change and partially lined by a Helmholtz resonator liner. Each duct is located between two axial coordinates $z_R$ and $z_L$ with the radius $a = R = 0.075$ m in the case of narrowing section [Figure 1(a)] and $a = \rho = 0.055$ $m$ in the case of widening at these positions [Figure 1(b)]. The radius change is defined by $e = R\text{-}\rho = 0.02$ m. Six configurations of ducts are studied, which differs according to the type of variation of discontinuity and position of the liner:

For the case of duct presenting radius narrowing [Figure 1(a)], three configurations are studied which differ with respect to the type of discontinuities and the position of the liner:

A-1 $\alpha = \frac{\pi}{2}$, $f = 0$ sudden narrowing and the part $c$ is lined, $L = b + c + b$ with $b = 0.35$ m and $c = 0.3$ m.

A-2 $\alpha < \frac{\pi}{2}$, $f \neq 0$ progressive narrowing and the part $c$ is lined; $L = b + f + c + f + b$ with $b = c = f = 0.2$ m.

A-3 $\alpha = \frac{\pi}{2}$, $f = 0$ sudden narrowing and the part $b_2$ is lined, $L = c_1 + c_2 + c_1 + c + \mathrm{b}$ with $c_1 = c_2 = c = b = 0.2$ m.

For the case of duct presenting widening of the radius [Figure 1(b)], three configurations are studied which differ with regard to the type of discontinuities and the position of the liner:

B-1 $\alpha = \frac{\pi}{2}$, $f = 0$ sudden widening and c is lined; $L = b + c + b$ with $b = 0.35$ m and $b = 0.3$ m.

B-2 $\alpha < \frac{\pi}{2}$, $f \neq 0$ progressive widening and c is lined; $L = b + f + c + f + b$ with $b = c = f = 0.2$ m.

B-3 $\alpha = \frac{\pi}{2}$, $f = 0$ sudden widening and $b_2$ is lined. The length of the duct will be as follows $L = c_1 + c_2 + c_1 + c + b$ with $c_1 = c_2 = c = b = 0.2$ m.

**Figure 1** Geometries of symmetric part of studied ducts

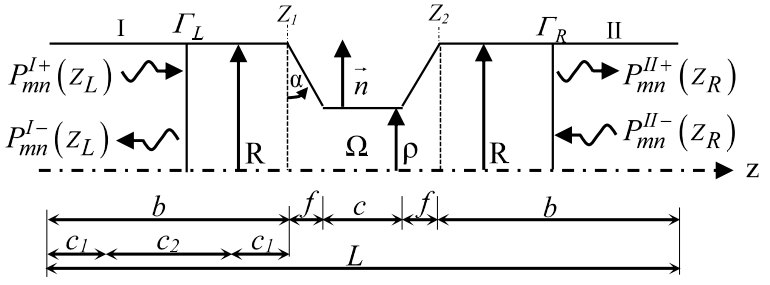


(a)

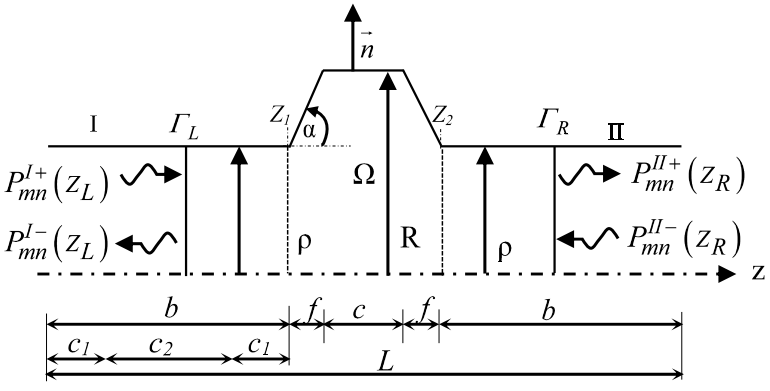


(b)

The acoustic liner is composed of a perforated plate backed by an air cavity and a rigid wall plate. It is characterised by its acoustic impedance $Z$, which is supposed to be locally reacting. The acoustic impedance of the liner is expressed as:

$$Z = Z_{perforated\ plate} + Z_{cavity} \tag{1}$$

$Z_{cavity}$ is the air cavity impedance expressed as:

$$Z_{cavity} = -jZ_0 \coth\left(kL_c\right) \tag{2}$$

$Z_0 = \rho_0 c$ is the characteristic impedance of the air, $\rho_0$ is the density of air, $c_0$ is the sound celerity in the air, $k$ is the acoustic wave number and $L_c$ is the air cavity depth. The acoustic impedance of the perforated plate is computed using the Elnady and Boden (2003) model:

$$\begin{aligned} Z_{Perforated\ Plate} = \mathrm{Re}&\left\{\frac{ik}{\sigma_p C_D}\left[\frac{t}{F\left(k_s' d_p/2\right)}+\frac{\delta_{re}}{F\left(k_s d_p/2\right)}\right]\right\} \\ &+ i\,\mathrm{Im}\left\{\frac{ik}{\sigma_p C_D}\left[\frac{t}{F\left(k_s' d_p/2\right)}+\frac{\delta_{im}}{F\left(k_s d_p/2\right)}\right]\right\} \end{aligned} \tag{3}$$

with $C_D$ being the discharge coefficient, $d_p$ is the pore diameter, $t$ *i*s the plate thickness, $\sigma_p$ is the plate porosity, $\delta_e$ and $\delta_{im}$ are correction coefficients given as follows:

$$\delta_{re} = 0.2d_p + 200d_p^2 + 16000d_p^3 \quad \delta_{im} = 0.2856d_p \tag{4}$$

$$F\left(k_s d_p/2\right) = 1 - \frac{J_1\left(k_s d_p/2\right)}{k_s \frac{d_p}{2} J_0\left(k_s d_p/2\right)} \qquad F\left(k_s' d_p/2\right) = 1 - \frac{J_1\left(k_s' d_p/2\right)}{k_s' \frac{d_p}{2} J_0\left(k_s' d_p/2\right)} \tag{5}$$

$$k_s' = \sqrt{\frac{-i\omega}{\nu'}} \qquad k_s = \sqrt{\frac{-i\omega}{\nu}} \tag{6}$$

where $\nu' = 2.179\frac{\eta}{\rho}$ is the kinematic viscosity.

## 3 Numerical computation of the multimodal scattering matrix

The multimodal scattering matrix $\boldsymbol{S}_{2N\times 2N}$ of the duct element located between the axial coordinates $z_L$ and $z_R$ relates the outcoming pressure waves array $\mathbf{P}_{2N}^{out} = \left\langle P_{00}^{I-}(z_L),...,P_{mn}^{I-}(z_L),P_{mn}^{II+}(z_L),...,P_{mn}^{II+}(z_L)\right\rangle_N^T$ to incoming pressure waves array $\mathbf{P}_{2N}^{in} = \left\langle P_{00}^{I+}(z_L),...,P_{mn}^{I+}(z_L),P_{mn}^{II-}(z_R),...,P_{mn}^{II-}(z_R)\right\rangle_N^T$ as follows (Taktak et al., 2010):

$$\mathbf{P}_{2N}^{out} = \mathbf{S}_{2N\times 2N} \times \mathbf{P}_{2N}^{in} \tag{7}$$

$P_{\mathrm{mn,}}^{\mathrm{I+}}\ P_{\mathrm{mn}}^{\mathrm{I-}}$ and $P_{\mathrm{mn,}}^{\mathrm{II+}}\ P_{\mathrm{mn}}^{\mathrm{II-}}$ are, respectively, the modal pressure coefficients associated to the ($m$, $n$) mode travelling, respectively, in the positive and the negative direction in both regions I and II (Figure 1). $m$ and $n$ are, respectively, the azimuthal and the radial mode numbers. $N$ is the number of propagating modes in both cross sections. The acoustic pressure $p$ in the duct is obtained by solving the Helmholtz equation with the boundary condition, respectively, at $\Gamma_{WD}$ with rigid wall duct and at $\Gamma_{LD}$ with lined duct part, characterised by acoustic impedance:

$$\begin{cases} \Delta p + k^2 p = 0 & (\Omega) \\ Z \dfrac{\partial p}{\partial n_{LD}} = i\omega\rho_0 p & \left(\Gamma_{LD}\right) \\ \dfrac{\partial p}{\partial n_{WD}} = 0 & \left(\Gamma_{WD}\right) \end{cases} \tag{8}$$

$\Delta$ is the Laplacien operator, $\Omega$ is the acoustic domain inside the duct, $n_W$ and $n_L$ correspond to normal vectors of each wall and $\omega$ is the pulsation.

To solve the system of equation (8), the finite element method is used. The corresponding weak variational formulation can be written as (Taktak et al., 2013):

$$\prod = -\int_{\Omega} (\nabla q.\nabla p)\, d\Omega + k^2 \int_{\Omega} qp d\Omega + \int_{\cup\Gamma_i} q \frac{\partial p}{\partial n_i} d\Gamma_i = 0, \tag{9}$$

where $q$ is the test function, $d\Omega$ and $d\Gamma_i$ are integration elements through the duct domain and boundaries, respectively, and $\cup\Gamma_i$ presents the whole boundary [$i$ = (Lined part) $LD$, (left) $L$, (right) $R$]. For this, the domain ($\Omega$) is discretised with triangular finite elements while edges are meshed by two-node finite elements. The computation of the integrals of equation (9) is made by the summation over the finite elements number of elementary integrals as presented in Taktak et al. (2012).

The last integral of this formulation (9) is given by the following expression, by adding the modal incoming and outcoming pressures as additional degrees of freedom to the model:

$$\int_{\cup\Gamma_i} q \frac{\partial p}{\partial n} d\Gamma = \int_{\Gamma_t} q\left(\frac{i\omega\rho p}{Z}\right) d\Gamma_{LD} + \sum_{n}^{N_r} ik_{mn} \begin{bmatrix} \left( n_L \left(P_{mn}^{I+} - P_{mn}^{I-}\right) \int_{\Gamma_L} qJ_m\left(\chi_{mn} r\right) d\Gamma_L \right) \\ + \left( n_R \left(P_{mn}^{II+} - P_{mn}^{II-}\right) \int_{\Gamma_R} qJ_m\left(\chi_{mn} r\right) d\Gamma_R \right) \end{bmatrix}, \tag{10}$$

where $J_m$ is the Bessel function of the first kind of order $m$, $\chi_{mn}$ is the $n^{\text{th}}$ root satisfying the radial hard-wall boundary condition on the wall of the main duct ($J'(\chi_{mn}/a) = 0$).

For a fixed $m$, system (8) results in the following matrix system, by taking into account the boundary conditions (Taktak et al., 2010).

$$\left[\left[q_1,\ldots,q_M\right],[1,\ldots,1]\right] \begin{bmatrix} \boldsymbol{K} & \boldsymbol{E}_1 & \boldsymbol{E}_2 & \boldsymbol{F}_1 & \boldsymbol{F}_2 \\ \boldsymbol{G}_1 & \boldsymbol{G}_2 & \boldsymbol{G}_3 & 0 & 0 \\ 0 & 0 & 0 & 0 & 0 \\ 0 & 0 & 0 & 0 & 0 \\ \boldsymbol{H}_1 & 0 & 0 & \boldsymbol{H}_2 & \boldsymbol{H}_3 \end{bmatrix} \begin{Bmatrix} \begin{Bmatrix} p_1 \\ \vdots \\ p_M \end{Bmatrix} \\ \left\{P_{mn}^{I-}\right\} \\ \left\{P_{mn}^{I+}\right\} \\ \left\{P_{mn}^{II-}\right\} \\ \left\{P_{mn}^{II+}\right\} \end{Bmatrix} = \begin{Bmatrix} 0 \\ \vdots \\ 0 \end{Bmatrix} \tag{11}$$

where $M$ is the node number in the domain $\Omega$, $\{p\}$ is the nodal acoustic pressure vector; $\boldsymbol{K}$ is a matrix relating the test function to the nodal pressures in the domain; $\boldsymbol{E}_1$, $\boldsymbol{E}_2$, $\boldsymbol{F}_1$ and $\boldsymbol{F}_2$ are matrices relating the test function to the modal pressures on $\Gamma_L$ and $\Gamma_R$; $\boldsymbol{G}_1$, $\boldsymbol{G}_2$ and $\boldsymbol{G}_3$ are matrices relating the nodal acoustic pressures in $\Omega$ to different modal pressures on the boundary $\Gamma_L$; $\boldsymbol{H}_1$, $\boldsymbol{H}_2$ and $\boldsymbol{H}_3$ are matrices relating the nodal acoustic pressures to different modal pressures on the boundary $\Gamma_R$. From this matrix system the total scattering matrix of the studied ducts is obtained.

## 4 Computation of the acoustic power attenuation

The acoustic power attenuation $W_{att}$ is defined as the ratio between the acoustic powers on both sides of the incoming waves $W^{in}$ and the outgoing waves $W^{out}$ (Taktak et al., 2010). It can also be deduced from the eigenvectors and eigenvalues of $\boldsymbol{H}$:

$$W_{att}(dB) = 10\log_{10}\left(W^{in}/W^{out}\right) = 10\log_{10}\left(\sum_{i=1}^{2N}|d_i|^2 \Big/ \sum_{i=1}^{2N}\lambda_i|d_i|^2\right) \tag{12}$$

with $d_i$ and $\lambda_i$ are the components and the eigenvalues of the matrix $\boldsymbol{H}$ defined as:

$$\begin{aligned}\boldsymbol{H}_{2N\times 2N} = &\left[\left[diag(XO)\right]_{2N\times 2N}\boldsymbol{S}_{2N\times 2N}\left[diag(XI)\right]^{-1}_{2N\times 2N}\right]^{T*}_{2N\times 2N}\\ &.\left[\left[diag(XO)\right]_{2N\times 2N}\boldsymbol{S}_{2N\times 2N}\left[diag(XI)\right]^{-1}_{2N\times 2N}\right]_{2N\times 2N}\end{aligned} \tag{13}$$

$$XI_{mn} = \sqrt{N_{mn}k^{+}_{mn}/2\rho_0 c_0 k} \quad XO_{mn} = \sqrt{N_{mn}k^{-}_{mn}/2\rho_0 c_0 k} \quad \{d\}_{2N} = \boldsymbol{U}^{T*}_{2N\times 2N}\{\Pi^{in}\}_{2N}$$

The acoustic power attenuation also depends on the scattering matrix of the duct element.

## 5 Numerical results

In this paper, the used liner is similar to the one used in Taktak et al. (2013). The parameters of this liner are as follows: plate thickness $t$ = 0.8 mm, hole diameter $d_p$ = 1mm, porosity $\sigma_p$ = 5%, air cavity depth $L_c$ = 20 mm. The acoustic impedance of this liner is then used as an input for the computation of the numerical multimodal scattering matrix of each studied configuration and therefore the acoustic power attenuation is calculated over the frequency range is $ka$ = [0–3.8] with $ka = \dfrac{\omega}{c}a$ is the non-dimensional wave number. The effect of four geometrical parameters of the liner and two parameters of the section change is evaluated by varying one of these parameters at a time while keeping others fixed.

**Figure 2** Effect of the length of the section change on the acoustic power attenuation of the three studied configurations (A-1), (A-2) and (A-3) of ducts having a radius narrowing

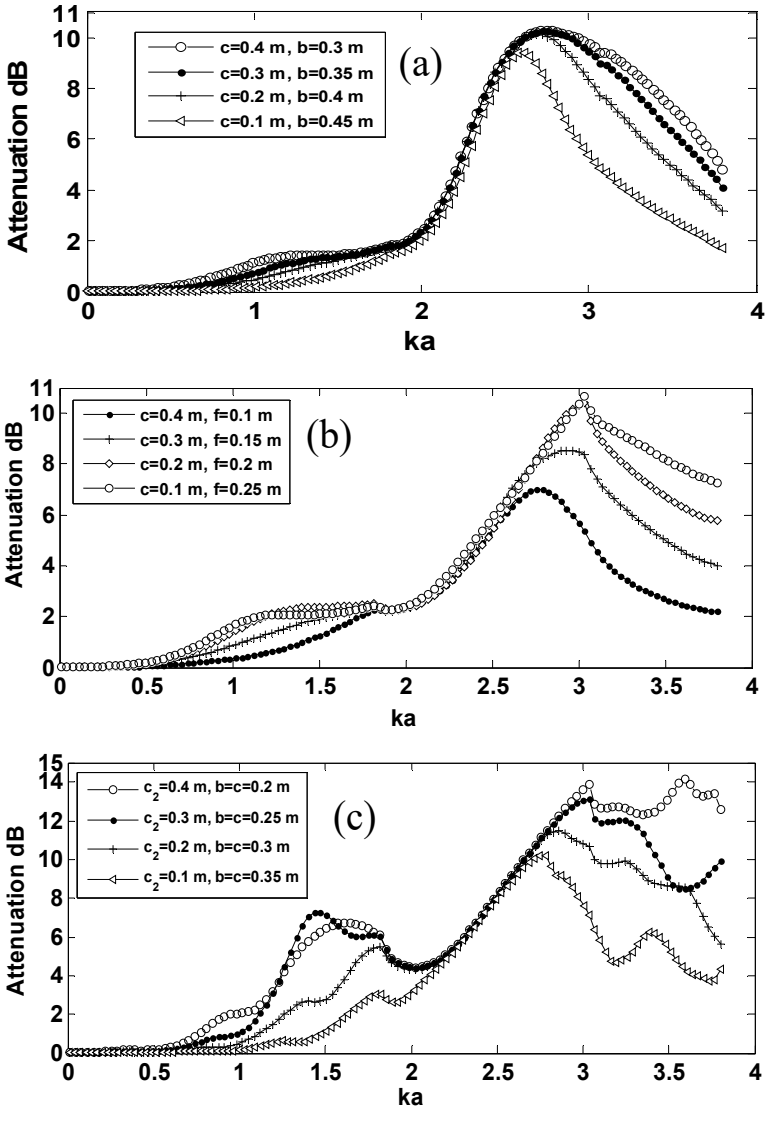

**Figure 3** Effect of the thickness e of the radius change on the acoustic power attenuation of the three studied configurations (A-1), (A-2) and (A-3) of ducts having a radius narrowing

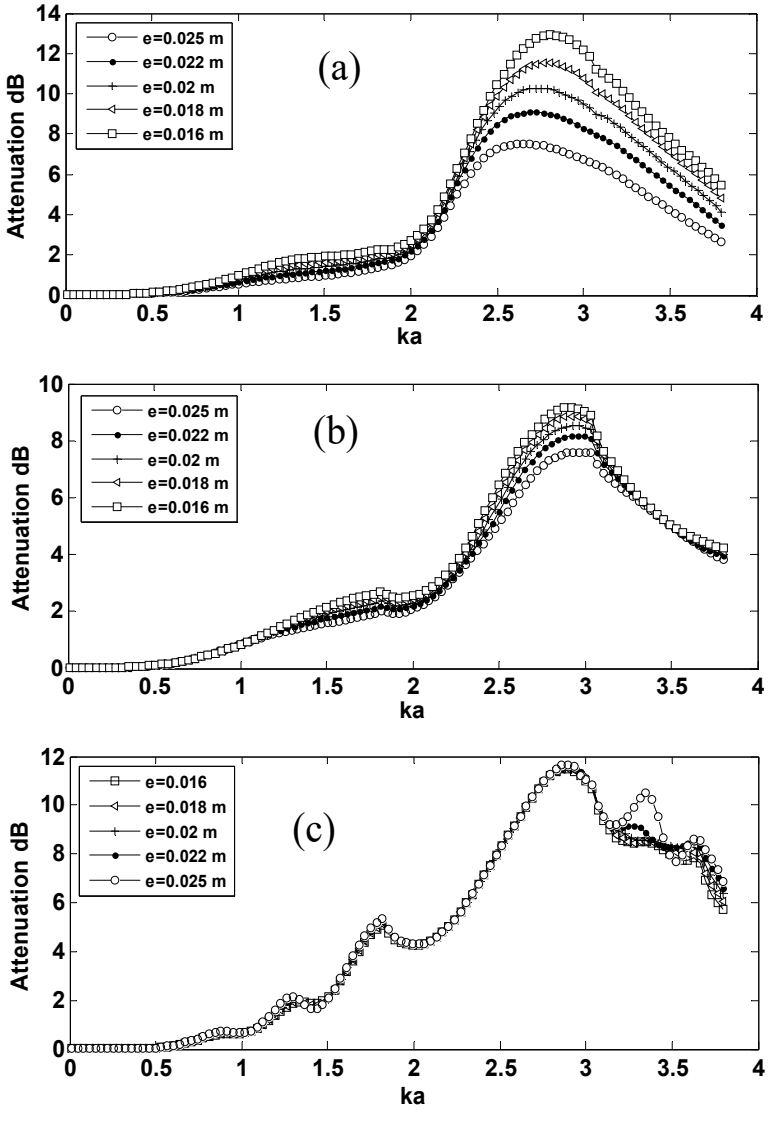

**Figure 4** Effect of the plate thickness *t* of the liner on the acoustic power attenuation for ducts of the three studied configurations (A-1), (A-2) and (A-3) of ducts having a radius narrowing

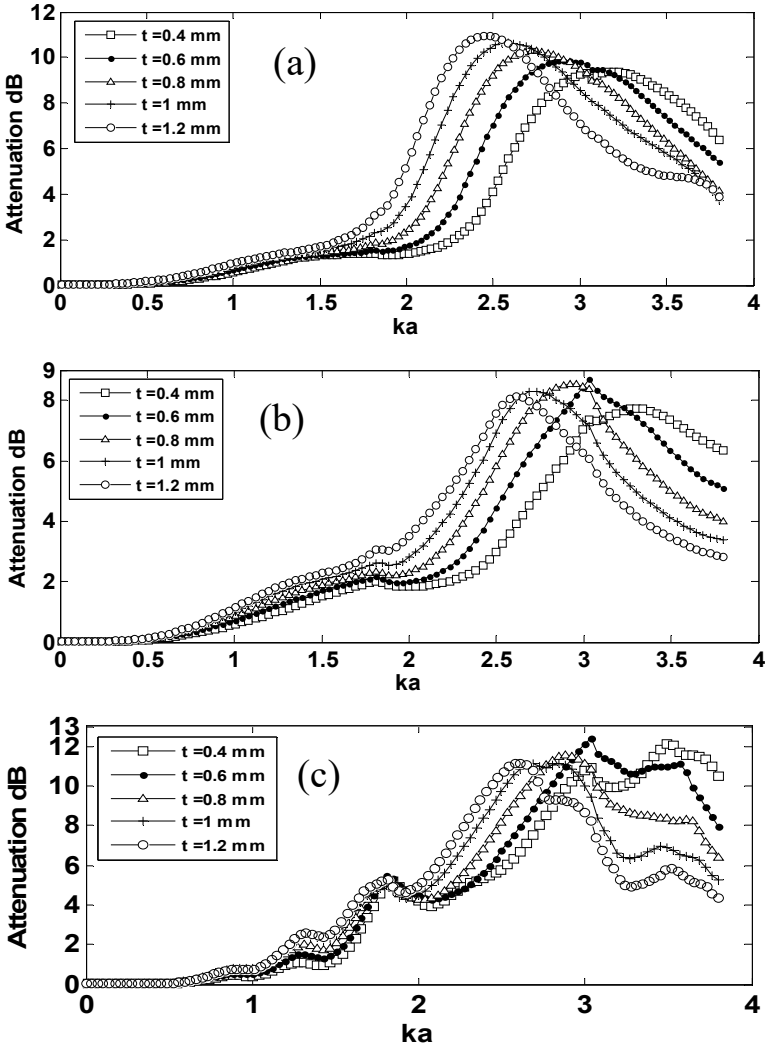


## *5.1 Configurations of ducts having a radius narrowing*

Figures 2(a), 2(b), 2(c) show the effect of the section length change on the acoustic power attenuation, respectively, for configurations (A-1), (A-2) and (A-3) versus the dimensional wave number *ka*. These figures reveal that this parameter does not have a significant effect on the acoustic power attenuation in the range of *ka* = [0.6–1.8] as indicated in Figure 2(b) also for *ka* below to 2.8 and 2.6 with very small variations which do not exceed 0.5 dB in the range of *ka* = [0.6–1.5] and 1 dB in the range of *ka* = [0.6–1.8], respectively, as illustrated in Figure 2(b) and 2(a). For other values of *ka*, the attenuation increases when the section change length increases as shown in

Figures 2(b) and 2(a). Conversely, in Figure 2(b), the attenuation rises as $c$ decreases. This is explained by the fact that the progressive discontinuity length $f$ increases and, therefore, produces a partial reflection of sound waves since, in this configuration, $c + 2f = 0.6$ m is taken into account. These figures show that the acoustic power attenuation starts to increase at $ka = 0.8$, however, this increase is negligible (< 1.65 dB) and (< 2.5 dB), respectively, in configurations (A-1) and (A-2) and then it presents a peak at high frequencies. Moreover, another rise in the attenuation is observed in the range of $ka$ = [0.8–2] in configuration (A-3), which increases with the increase of $c$ to reach 7.2 dB at $ka = 1.2$ for $c_2 = 0.3$ m. It can be seen that the amplitude and the frequency of the resonance peak are almost identical, about 10.16 at $ka = 2.7$, when varying the section change in Figure 2(a), however, this amplitude increases and shifts to higher frequencies in Figures 2(b) and 2(c), when the section change increases. The maximum of attenuation and the corresponding frequency vary as follows: from 7 dB at $ka = 2.75$ to 10.67 dB at $ka = 3.03$ and (10.21 dB at $ka = 2.75$ to 13.9 dB at $ka = 3.03$ and 14.1 dB at $ka = 3.6$, respectively, in configurations (A-2) and (A-2) and (A-3). According to these results, it can be seen that configurations (A-1) and (A-2) yield a close value of a maximum attenuation and the configuration (A-3) provides higher attenuation compared to other configurations and therefore it is more efficient. Figures 3(a), 3(b) and 3(c) display the effect of thickness $e$ on the acoustic power attenuation of the three studied configurations (A-1), (A-2) and (A-3) when varying this parameter from 0.016 m to 0.025 m. These figures show that this parameter does not have a significant effect in Figure 3(c), as well in Figure 3(b) with a small increase of the attenuation as the increase of $e$ is only in the range of $ka$ = [2.4–3.03] which does not exceed 2 dB (it passes from 7.6 dB to 9.1 dB at $ka = 2.9$) and for $ka$ below 2.4 in Figures 3(a). It can be observed that the acoustic power attenuation in each configuration varies similarly with respect to the three configurations in Figures 2(a), 2(b) and 2(c). Furthermore, the resonance peak grows slightly as $e$ increases in Figure 3(a) and the amplitude of this peak passes from 7.5 dB at $ka = 2.7$ to 12.9 dB at $ka = 2.8$. Moreover, the maximum of attenuation is equal to 11.8 dB at $ka$ =2.9 in configuration (A-3). We conclude that the resonant frequency and the frequency band of these configurations remain identical regardless $e$. This implies that resonance frequency is related to the radius of ducts. It is noticeable that configuration (A-1) provides a higher attenuation peak; therefore, it is more efficient. Figures 4(a), 4(b), 4(c) show the effect of the thickness $t$ of the liner on the acoustic power attenuation, respectively, for configurations (A-1), (A-2) and (A-3) versus $ka$. It is observed that the form of attenuation curves, in all studied configurations, are similar to that of the effect of thickness $e$ in Figures 4. It is also noticed that the attenuation peak grows slightly when $t$ increases in configuration (A-1) and it passes from (9.2 dB for $t = 0.2$ mm to 10.97 dB for $t = 1.2$ mm). Conversely, in Figure 4 (A-3) the maximum of attenuation passes from (11.1 dB *for* $t = 1$ mm to 12.5 dB for $t = 0.4$ mm) and it varies between 7.6 dB and 8.68 dB in configuration (A-2). A maximum of attenuation is better in configuration (A-3) than configurations (A-1) and (A-2), therefore, it is the most absorbent. Results reveal that this parameter does have not an important effect on the amplitude of attenuation peak, however, it has an effect on the resonance frequency that leads to pushing the attenuation peak to lower frequencies when t increases:

(A-1): $ka$ =3.2 for $t = 0.4$ mm to $ka$ =2.45 for $t = 1.2$ mm

(A-2): $ka$ =3.8 for $t = 0.2$ mm to $ka$ =2.6 for $t = 1.2$ mm

(A-3): *ka* =2.7 for *t* = 0.4 mm to *ka* =3.5 for *t* = 1 mm).

**Figure 5** Effect of the perforation diameter $d_p$ of the liner on the acoustic power attenuation of the three studied configurations (A-1), (A-2) and (A-3) of ducts having a radius narrowing

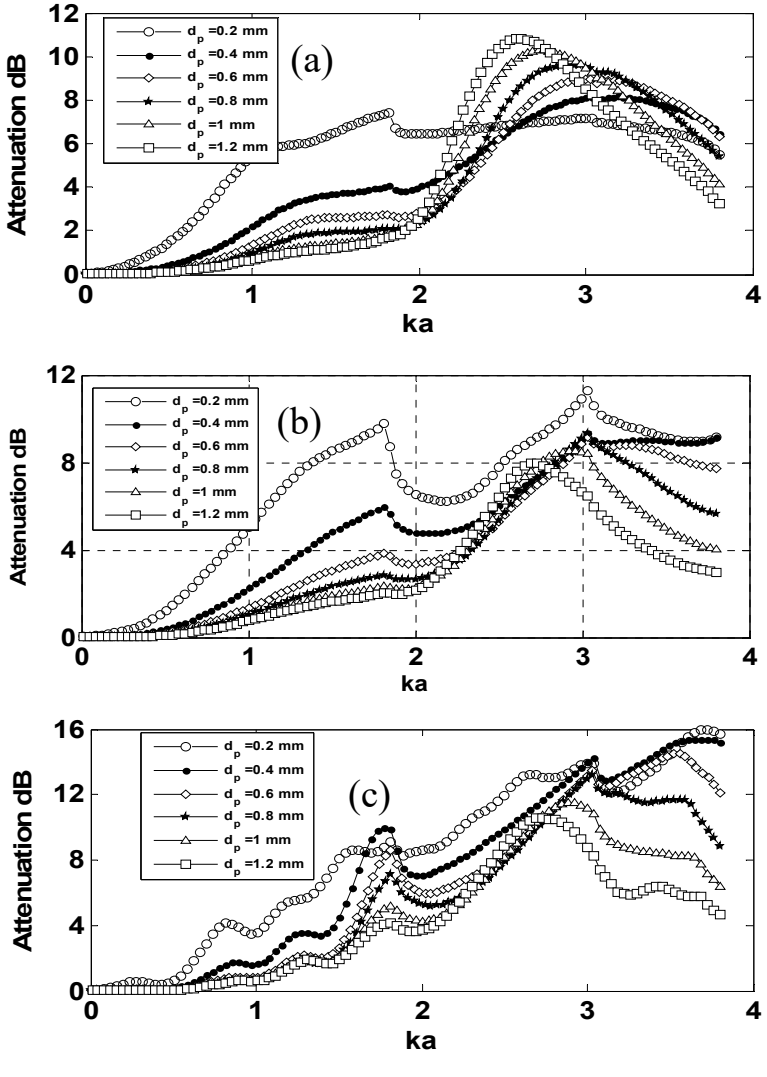

**Figure 6** Effect of the air cavity depth $L_c$ of the liner on the acoustic power attenuation of the three studied configurations (A-1), (A-2) and (A-3) of ducts having a radius narrowing

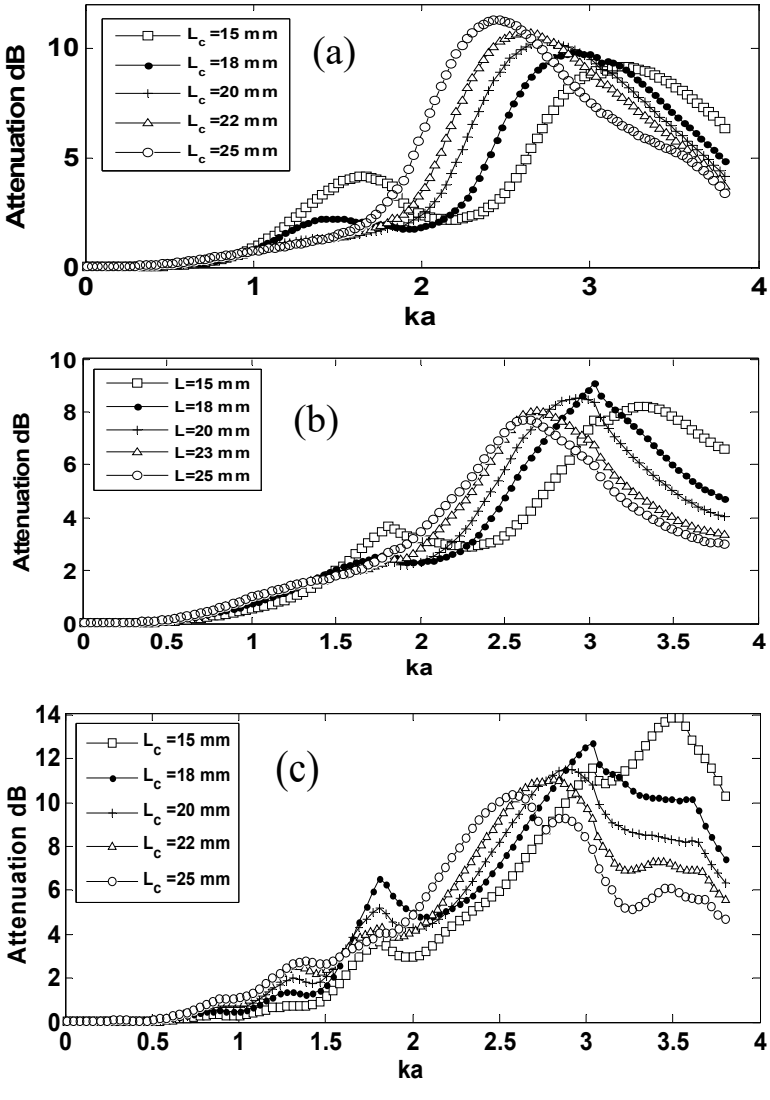

**Figure 7** Effect of porosity $\sigma_p$ [%] of the liner on the acoustic power attenuation of the three studied configurations (A-1), (A-2) and (A-3) of ducts having a radius narrowing

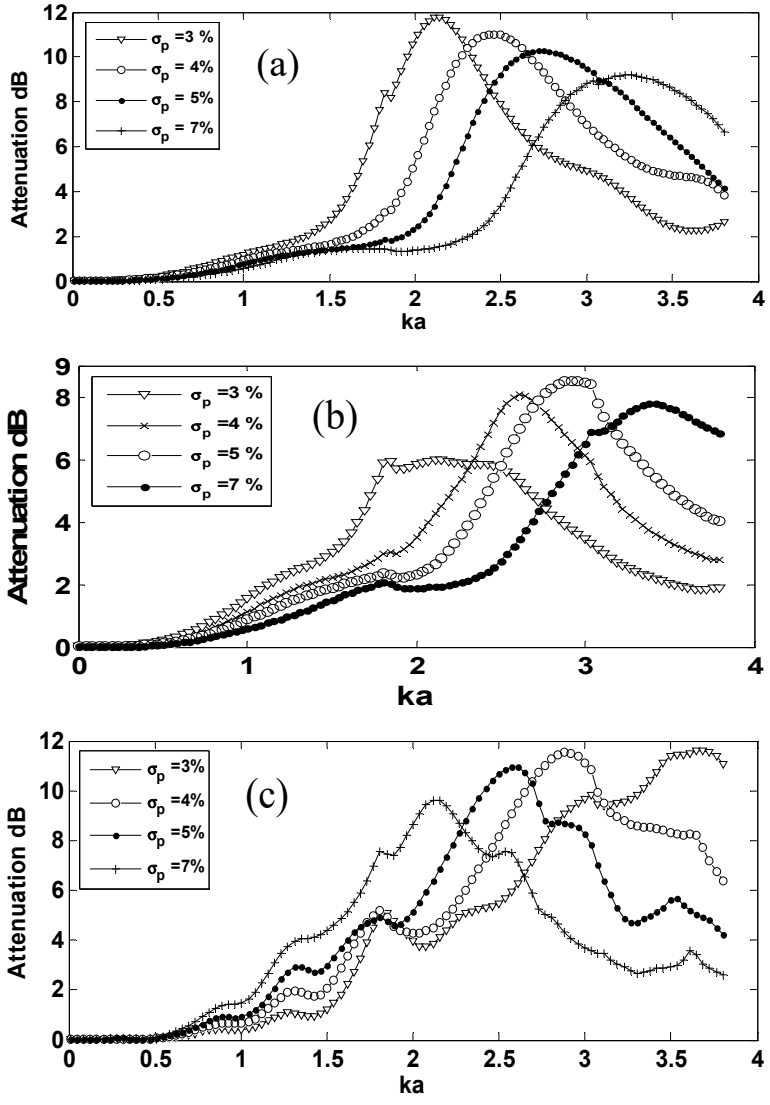


The observed effect is elucidated by the fact that the mass of air contained in the perforation is more important when the plate is thicker and the frequency of resonance decreases. The acoustic resistance increases with *t*. This is explained by the fact that the thermal and viscous boundary layers in the perforations are present on a larger surface. The acoustic dissipation is, therefore, more important. Figures 5(a), 5(b) and 5(c) exhibit the effect of the perforation diameter of the liner on the acoustic power attenuation of configurations (A-1), (A-2 and (A-3), respectively. These figures show that the effect of

this parameter is important. It is noted, in each configuration, that the attenuation grows as a function of *ka* for diameter varying from 0.2 to 0.4 mm with drops observed in Figure (A-2) and fluctuations in Figure (A-3). It is noteworthy that the attenuation resonance phenomenon appears only for the wider diameter $d_p$=1, 1.2, ($d_{p>t}$) because the wave acoustic can be penetrated better inside the plate, which is contrary to small values diameter, where the wave acoustic cannot penetrate into the plate and therefore will be reflected. Decreasing $d_p$ from 1.2 mm to 0.2 mm generates an increase of the acoustic power attenuation in configurations (A-2) and (A-c) and only for *ka* below 2 in configuration (A-1) which presents a slight decrease in the amplitude of attenuation peak from 10.27 dB, *ka* = 2.75 to 10.8, *ka* = 2.6 for a diameter equal to 1 and 1.2 mm, respectively, as well as a very slight increase of the attenuation when $d_p$ increases from 0.2 to 0.4 mm at *ka* above 2.6. The maximum of attenuation and the corresponding frequency vary in each configuration as; ((A-2): 7.95 dB at *ka* = 2.8 to 11.28 dB at *ka* = 3.03; (A-c): 10.6 dB at *ka* = 2.7 to 17.24 dB at *ka* =3.8). It can be noticed that configuration (A-3) is more efficient than other configurations, particularly at a higher frequency. Figures 6(a), 6(b) and 6(c) represent the effect of air cavity depth $L_c$ on the acoustic power attenuation versus *ka*, respectively, for configurations (A-1), (A-2) and (A-3). These figures reveal that the attenuation behaviour in each configuration is similar to that of the effect of thickness t in Figures 5 (A-1), (A-2), and (A-3). It can be seen that the resonant frequency is reduced by increasing $L_c$ and it varies in each configuration as follows: ((A-1): *ka* = 3.2 for $L_c$ = 15 mm to *ka* = 2.46 for $L_c$ = 25 mm; (A-2): *ka* = 3.34 for $L_c$ = 15 mm to *ka* = 2.6 for $L_c$ = 25 mm; (A-3): *ka* = 3.5 for $L_c$ = 25 mm to *ka* = 2.6 for $L_c$ = 25 mm). Moreover, the amplitude of the resonance peak rises with the increase of $L_c$ in configuration (A-1) and it passes from 9.1 dB for $L_c$ = 25 mm to 11.2 dB for Lc = 15 mm. Conversely, in Figure (A-c), this amplitude grows as $L_c$ decrease and it passes from 10.35 dB for $L_c$ = 25 mm to 13.88 dB for $L_c$ = 15 mm. However, the amplitudes of attenuation peaks in configuration (A-2) are close and they vary between 7.7 dB and 9 dB. These results display that configuration (A-3) provide a good attenuation at a higher frequency, thus being the most efficient. Figures 7(a), 7(b) and 7(c) show the effect of the porosity σp on the acoustic power attenuation versus ka for the three studied configurations (A-1), (A-2) and (A-3). They display an important effect of this parameter. It can be observed that the attenuation presents a resonance peak in each configuration, whose amplitude of this peak slightly increases when $\sigma_p$ increases, as shown in Figures 7(A-1) and (A-3), however, it varies inversely in Figure 7 (A-2). On the other hand, the resonant frequency rises with the increase of σp, as presented in figure 7 (A-1) and (A-2), and it varies inversely in Figure 7 (A-2). The maximum of attenuation and the corresponding frequencies pass from each configuration as follows: ((A-1): 9.2 dB, *ka* = 3.2 for $\sigma_p$ = 7% to 11.75 dB for $\sigma_p$ = 3%, *ka* = 2.14; (A-2): 8.1 dB, *ka* = 1.08 for $\sigma_p$ = 1% to 6 dB, *ka* =2.1 for $\sigma_p$ = 7% to 7.77 dB, *ka* = 3.4 for $\sigma_p$ = 7%; (A-3): 9.6 dB, *ka* = 2.1 for $\sigma_p$ = 7% to 11.6 dB, *ka* = 3.68 for $\sigma_p$ = 3%). It can be seen that the resonance frequency increases as $\sigma_p$ increases, as indicated in Figures 7(a) and 7(b), however, in Figure 7 (c), results show that configuration (A-3) yields a better attenuation at high frequencies region, while configuration (A-1) can be more efficient at a lower frequency.

**Figure 8** Effect of the length of the section change on the acoustic power attenuation of configuration for ducts of the three studied configurations (B-1), (B-2) and (B-3) of ducts having a radius widening

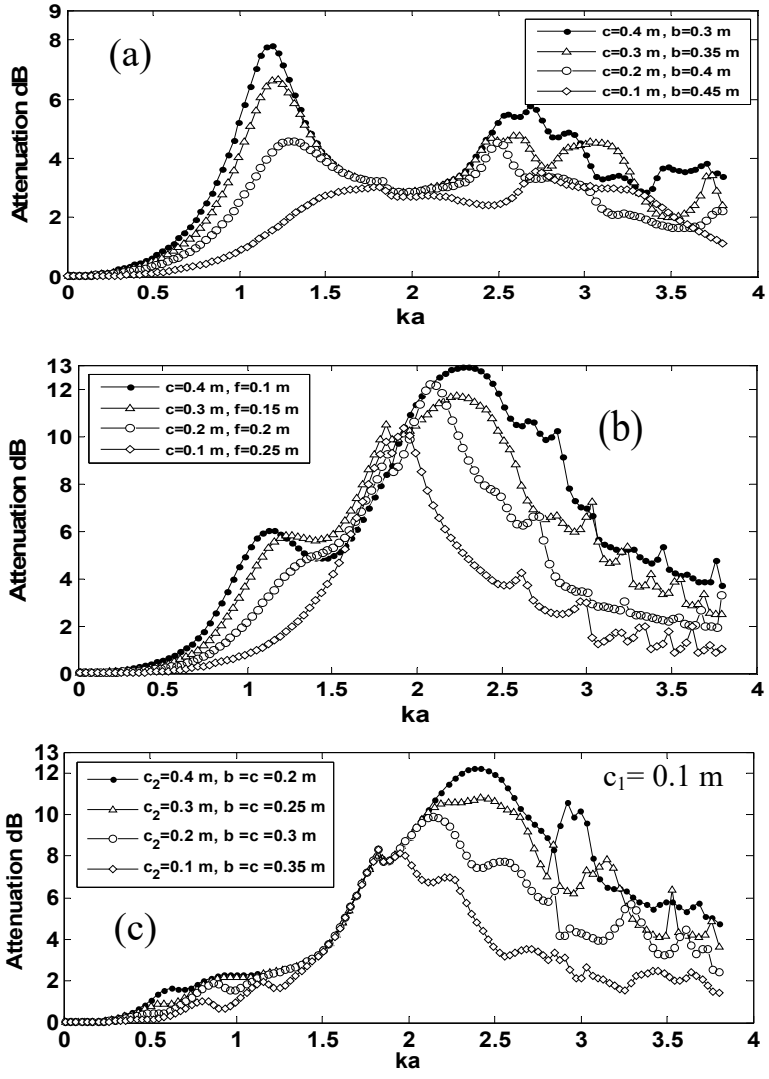

**Figure 9** Effect of the thickness *e* of the section change on the acoustic power attenuation of the three studied configurations (B-1), (B-2) and (B-3) of ducts having a radius widening

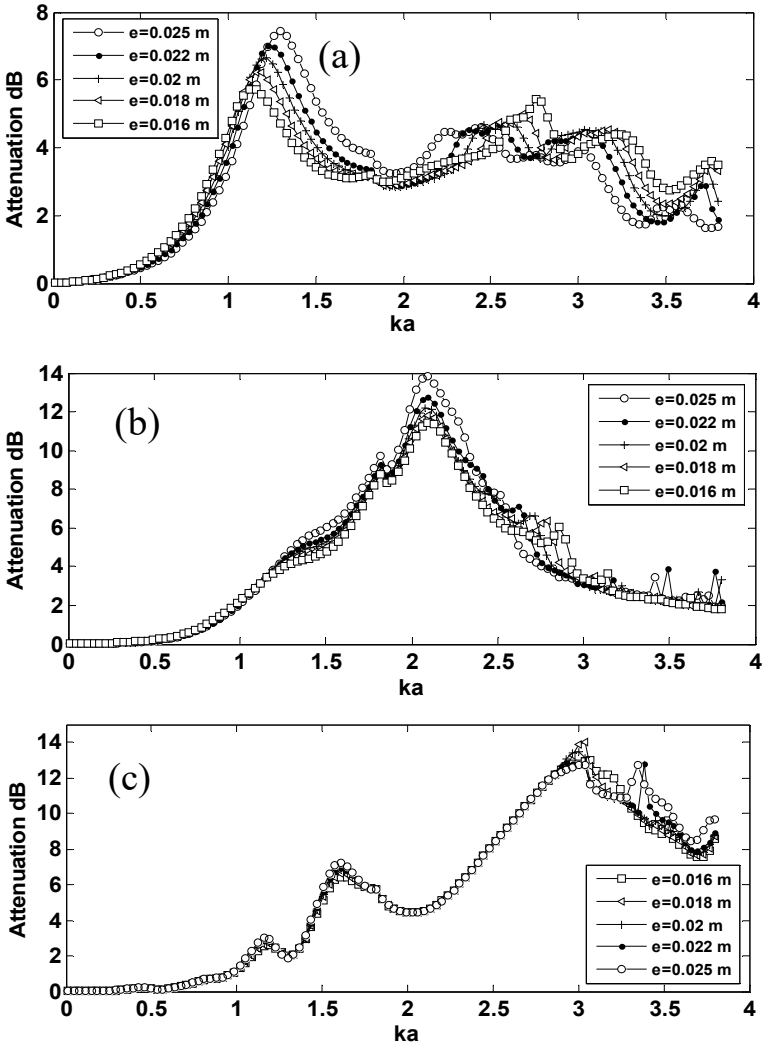

**Figure 10** Effect of the thickness *t* of the liner on the acoustic power attenuation of ducts having a radius widening of the three studied configurations (B-1), (B-2) and (B-3)

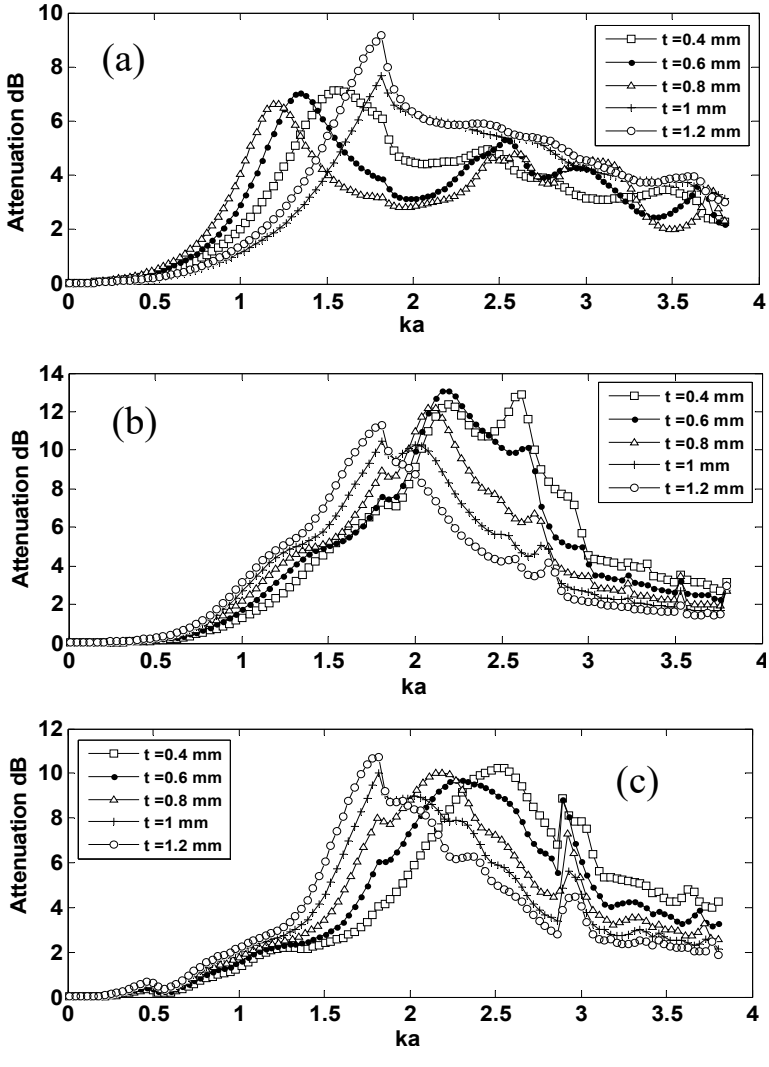

**Figure 11** Effect of the perforation diameter $d_p$ of the liner on the acoustic power attenuation of the three studied configurations (B-1), (B-2) and (B-3) of ducts having a radius widening

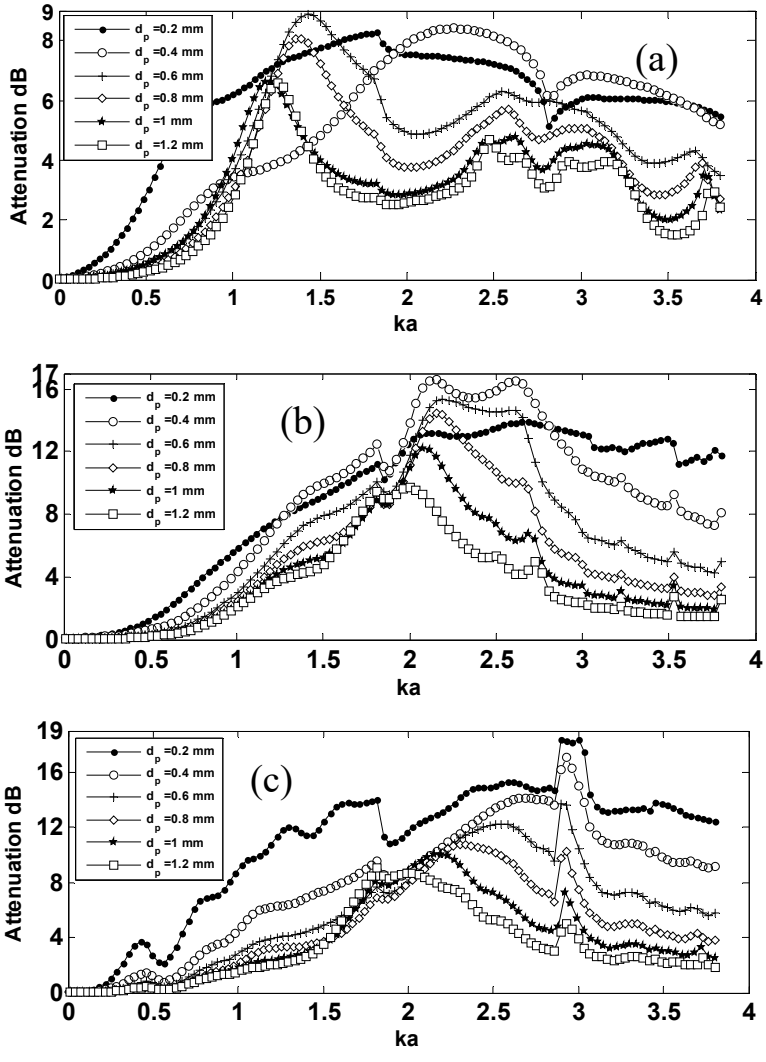

**Figure 12** Effect of the porosity $L_c$ of the liner on the acoustic power attenuation of the three studied configurations (B-1), (B-2) and (B-3) of ducts having a radius widening

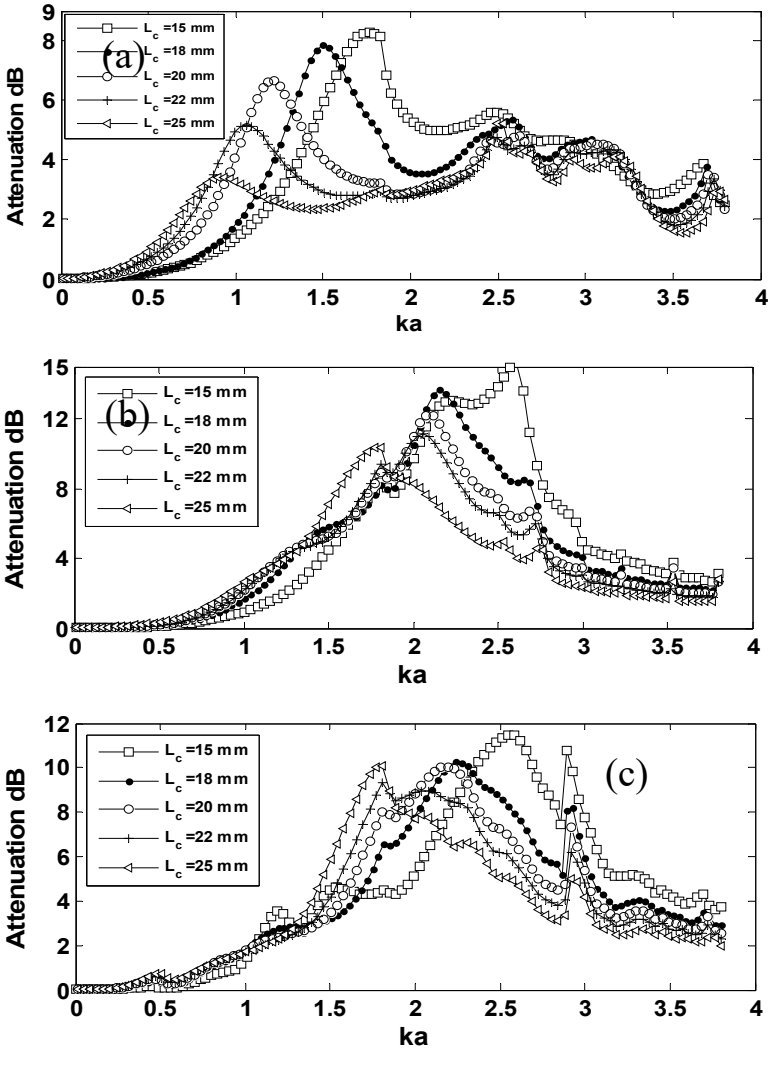

**Figure 13** Effect of the porosity $\sigma_p$ of the liner on the acoustic power attenuation of the three studied configurations (B-1), (B-2) and (B-3) of ducts having a radius widening

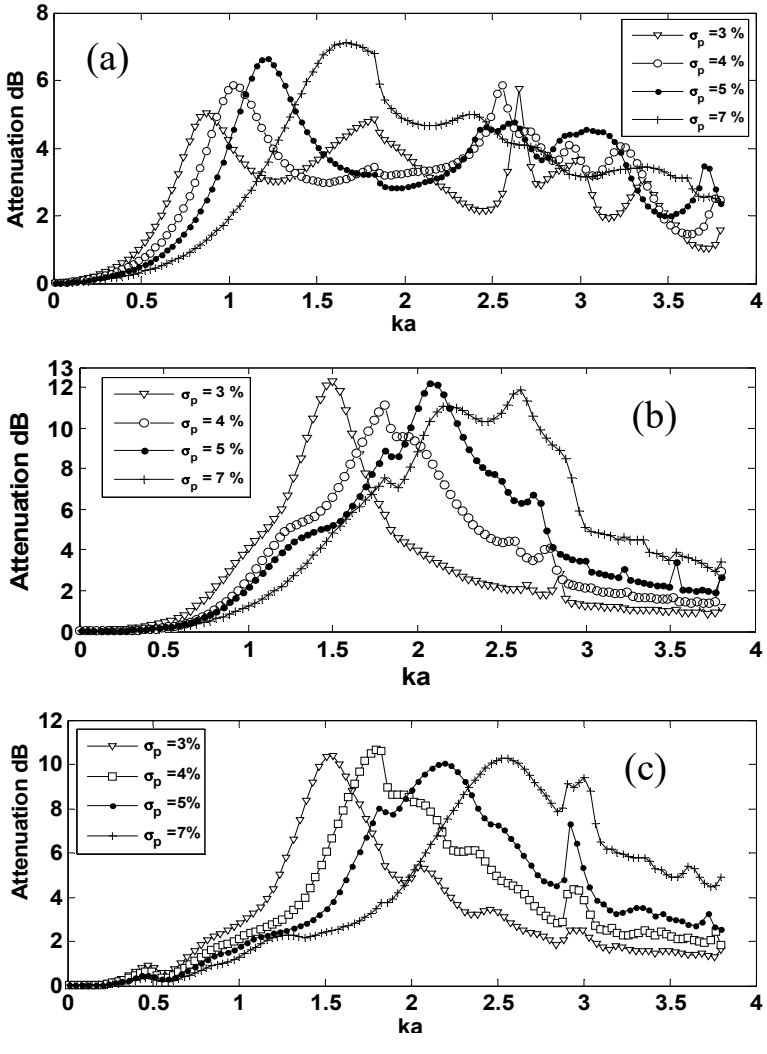

### 5.2 Configurations of ducts having a radius widening

Figures 9(a), 9(b), 9(c) show the effect of the section change length on the acoustic power attenuation, respectively, for configurations (B-1), (B-2) and (B-3) versus *ka*. These figures reveal that the form attenuation curves change and are disturbed for higher frequency in all three studied configurations compared to Figures 3(a), (b), and (c) (in the case of the narrowing of radius in duct). It can be seen that the attenuation is nil for *ka* below 0.5 and then it shows a peak with larger band in figures (b) and (c). Besides, in Figure 9(a), the attenuation presents a peak in *ka* = [0.5–1.5] with narrower band and then it decreases to reach 2.83 dB at *ka* =2.8 where it slightly rises and again decreases. By increasing the section change length the attenuation peak increases in three configurations, however, there is no significant effect for *ka* = [1.5–2.4] in Figure 9(a) and for *ka* below 2 in Figure 9(c). The maximum of attenuation and the corresponding frequency differ in each figure and they are about 8.3 dB, *ka* =1.1; 12.93 dB, ka=2.3; 12.2 dB, *ka* = 2.4, respectively, for configurations (a), (b) and (c). Based on these results, configuration (B-1) is good in low frequency and configurations (B-2) and (B-3) are better in medium frequency, while configuration (A-3) of duct, having narrowing radius, is the most efficient, particularly, at higher frequency. The effect of the variation of thickness *e* on the acoustic power attenuation for three configurations of ducts, having widening radius, is presented in Figures 10(a), 10(b) and 10(c). They show there are no significant effect of *e* in Figures 10 (a) and (c) and a small increase of the attenuation as *e* increases in the range of *ka* = [1–1.6], which does not exceed 2dB in Figure 10 (a). It can be observed that the attenuation behaviour in Figures 10 (c) is similar to Figure 3 (c) in the case of ducts having narrowing radius, as well as in Figures 10 (b), however, the attenuation peaks are shifted to *ka* = 2.2. On the other hand, the attenuation behaviour of Figures 10 (a) is similar to effect of the length *c* in Figure 9 (a). A maximum of attenuation and the corresponding frequency are about 7.4 dB, *ka* =1.2; 13.8 dB, *ka* =2; 14 dB *ka* =3.03, respectively, for configurations (a), (b) and (c).Therefore, configuration (B-3) is the most efficient, particulary, at high frequency compared to all studied configurations. Besides, configuration (B-2) is quiet good at medium frequency. Figures 11(a), 11(b) and 11(c) present the effect of thickness *t* , in the case of ducts having a radius widening. Figures 11(a), 11(b) and 11(c) display the effect of the thickness *t*, in the case of ducts having a radius widening. They show that the attenuation starts to increase at *ka* = 0.6 and present a perturbation at higher frequencies. Figure 11 (a) reveals that the attenuation presents a peak with a narrow band for *ka* varying from 0.5 to 1.5, then it decreases very slightly to reach 2 to 3 dB. It is observed that the frequency of the peak attenuation grows for *ka* varying from 1.3 to 1.6, when thickness *t* passes from 0.2 mm to 0.8 mm, being located at *ka* =1.7 for *t* = 1, 1.2 mm. Figures 11(b) and 11(c) demonstrate a significant increase of attenuation peaks, which shifts towards higher frequencies as well as an increase in the frequency band where *ka* varies from 0.5 to 3, compared to figure (a). Moreover, the frequency of attenuation peak grows as *t* is reduced and it passes from *ka* =1.8, *t* = 1.2 mm to *ka* =2.8, *t* = 0.4 mm. A maximum of attenuation peak is about 9.1 dB; 13.1 dB; 10.7 dB, respectively, for configurations (B-1), (B-2) and (B-3). The attenuation peak performance is better in configuration (B-2). Figures 12 (A-1), (A-2), and (A-3) show very interesting results with regards to the effect of the diameter in the three studied configurations of ducts, having a widening radius. It can be seen that the effect of $d_p$ in Figure 12 (B-3) is similar to that of Figure 5 (B-3). Figure (B-2) show that the attenuation presents a resonance peak with large frequency

band for *ka* varying from 0.6 to 3.03, except that for $d_p$ = 0.2 which rises to final point when *ka* increases. The resonant frequency shifts to higher frequency with the decrease of $d_p$. However, Figure (B-1) exhibits an increase of the attenuation when *ka* increases, to reach a maximum and then it decreases with small drops observed at *ka* = 1.9 and *ka* = 2.9, except for $d_p$ = 1, 1.2 mm, which presents a peak. Moreover, the attenuation rises when $d_p$ decreases and it varies in each configuration as follows: ((B-1) 8.2 dB, *ka* = 2.3 to 7.6 dB, *ka* =1.7; (B-2): 9.7 dB, *ka* = 2 to 16.5 at *ka* = 2.1; (B-3): 9.1 dB to 14.05 at *ka* = 1.8 and 5 dB to 18.2 dB at *ka* =2.9). Accordingly to these results, configuration (B-2) with $d_p$ = 0.4 mm provides better performance of attenuation peak and a larger frequency band, thus it is the most efficient. Figures 13 (a), (b) and (c) display the effect of $L_c$ in the case of ducts having a radius widening for the three studied configurations. It can be seen that the variation of attenuation is similar to that the thickness t in Figures 10 (a), (b) and (c). The amplitudes and the positions of the attenuation peaks are different compared to those of the three configurations of ducts having narrowing radius in Figures 5 (a), (b) and (c): the more the cavity is thin, the more the attenuation peak is shifted to the higher frequencies. Moreover, it is observed that the amplitude of the attenuation peak grows when $L_c$ is reduced, as shown in Figures (a) and (b), however, it remains almost in the same level in Figure (c). The amplitude and the frequency of attenuation peak vary in each configuration as follows: ((B-1): 3.4 dB, *ka* = 0.9 for $L_c$ =25 mm to 8.2 dB, *ka* =1.76 for $L_c$ =15 mm; (B-2): 10.36 dB, *ka* =1.8 for $L_c$ = 25 mm to 15.04 dB, *ka* =2.6 for $L_c$ =15 mm; (B-3): 10.1 dB, *ka* =1.8 for $L_c$ =25 mm to 10.25 dB, *ka* =2.2 for $L_c$ =15 mm). Thus, it is concluded that configuration (B-2) is the most efficient. The effect of $\sigma_p$ on the acoustic power attenuation for the three studied configurations of ducts having radius widening are plotted, respectively, in Figures 14(a), 14(b) and 14(c). They show that the frequency of attenuation peaks are slightly shifted towards lower frequency with small perturbations, observed for higher frequency, when compared to the three configurations of the case of narrowing ducts. The frequency of resonance peak increases when $\sigma_p$ increases and it varies in each configuration as follows: ((B-1): *ka* =0.87 for $\sigma_p$ =3% to *ka* = 1.66 for $\sigma_p$ = 7%; (B-2) *ka* =1.5 for $\sigma_p$ =3% to *ka* =2.6 for $\sigma_p$ =7%; (B-3): *ka* =1.5 for $\sigma_p$ = 3% to *ka* =2.5 for $\sigma_p$ = 7%). Moreover, the maximum of attenuation rises as $\sigma_p$ increases in Figure (a) and it passes from 5 dB for $\sigma_p$ =3% to 7.1dB for $\sigma_p$ =7%. However, it is almost closer in configurations (B-2) and (B-3), having a maximum of attenuation equal to 12.26 dB and 10.35 dB, respectively. It can be noticed that configuration (B-2) provides a greater attenuation compared to all studied configurations and, therefore, it is the most efficient.

## 6 Conclusions

This study was conducted to identify the influential parameters of the liner and geometries as well as their acoustic performance on the acoustic power attenuation of lined ducts with various configurations by using the scattering matrix method. This work is realised for six configurations of ducts discontinuities which differ on type discontinuity and lined-part position. The following primary conclusions are drawn from the results of this study:

- The liner parameters are highly influenced by the type of section change on each lined duct. In the case of ducts having a narrowing radius, configuration (A-3) yields a better performance of liner characteristics on the attenuation peak and the frequency band; however, it is slightly disturbed. In the case of ducts having a widening radius, evanescent modes are generated at the level of discontinuities in the case of ducts having a widening radius and even if they are quickly attenuated in some frequency, their effects cause disturbances for higher frequencies. Configuration (B-2) provides a better performance of liner characteristics on the attenuation peak and the frequency band. Furthermore, it is noticeable that configuration (B-1) is good at low frequency, configuration (B-2) is better at medium frequency and configuration (B-3) is the best choice for higher frequency, as well as the case of narrowing radius of duct.
- The plate thickness $t$, the porosity $\sigma_p$ and the length of cavity $L_c$ strongly influence the resonance frequency and therefore allow fixing their position. However, the diameter $d_p$ has an influence on the maximum of attenuation.

## References

Akoum, M. and Ville J.M., (1998), Measurement of reflection matrix of a discontinuity in a duct. *Journal of the Acoustical Society of America*, Vol. 103, No. 5, pp.2463–2468.

Ben Jedidia, M., Akrout, M., Taktak, M., Hammami, L. and Haddar, M. (2016) 'Thermal effect on the acoustic behavior of an axisymmetric lined duct', *Applied Acoustics*, Vol. 86, pp.138–145.

Demir, A. (2016) 'Sound transmission in a duct with sudden area expansion, Extended Inlet and lined walls in overlapping region', *Advances in Acoustic and Vibration*, Vol. 2016, Article ID 948516.

Demir, A. (2017) 'Scattering matrices in non-uniformly lined ducts', *Zeitschrift für angewandte Mathematik und Physik*, Vol. 68, No. 1, pp.1–15.

Dhief, R., Makni, A., Taktak, M., Chaabane, M. and Haddar, M. (2020) 'Investigation on the effects of acoustic liner variation and geometry discontinuities on the acoustic performance of lined ducts', *Archives of Acoustics*, Vol. 45, No. 1, pp.49–66.

Elnady, T. and Boden, H. (2003) 'On semi-empirical liner impedance modelling with grazing flow', *Proceedings of 9th AIAA/CEAS Aaeroacoustics Conference*, USA.

Homentcovschi, D. and Miles, R.N. (2010) 'A re-expansion method for determining the acoustical impedance and the scattering matrix for the waveguide discontinuity problem', *Journal of the Acoustical Society of America*, Vol. 128, No. 2, pp.628–638.

Knobloch, K., Enghardt, L. and Bake, F. (2018) 'Helmholtz resonator liner with flexible walls', *Proceedings of the 24th AIAA/CEAS Aeroacoustics Conference*, Georgia, USA, Paper No 2018-4102, June.

Martin, D. and Michael, K. (2018) 'Experimental study of advanced Helmholtz resonator liners with increased acoustic performance by utilizing material damping effects', *Applied Sciences*, Vol. 8, No. 10, pp.1–18.

Masmoudi, A., Makni, A., Taktak, M. and Haddar, M. (2017) 'Effect of geometry and impedance variation on the acoustic performance of a porous material lined duct', *Journal of Theoretical and Applied Mechanics*, Vol. 55, No. 2, pp.679–694.

Miles, J.W. (1946) 'The analysis of plane discontinuities in cylindrical tubes', *Part I, Journal of the Acoustical Society of America*, Vol. 17, No. 3, pp.259–271.

Ni, F., Miguel-Brebion, M., Nicoud, F. and Poinsot, T. (2017) 'Accounting for acoustic damping in a 3D Helmholtz solver', *ICSV*, Vol. 24, 23–27 July.

Othmani, C., Hentati, T., Taktak, M., Elnady, T., Fakhfakh, T. and Haddar, M. (2015) 'Effect of liner characteristics on the performance of duct systems', *Archives of Acoustics*, Vol. 40, No. 1, pp.117–127.

Peat, K.S. (1988) *The Acoustical Impedance at Discontinuities of Ducts in the Presence of a Mean Flow*, Department of Engineering Mathematics, University of Technology, Loughborough, Leicestershire, England.

Sitel, A., Ville, J.M. and Foucart, F. (2003) 'An experimental facility for measurement of acoustic transmission matrix and acoustic power dissipation of duct discontinuity in higher order modes propagation conditions', *Acta Acustica United Acustica*, Vol. 89, No. 4, pp.586–594.

Sitel, A., Ville, J.M. and Foucart, F. (2006) 'Multimodal procedure to measure the acoustic scattering matrix of a duct discontinuity for higher order mode propagation conditions', *Journal of the Acoustical Society of America*, Vol. 120, No. 5, pp.2478–2490.

Taktak, M., Majdoub, M.A., Bentahar, M. and Haddar, M. (2012) 'Numerical modelling of the sound propagation in axisymmetric lined flow duct', *Archives of Acoustics*, Vol. 37, No. 2, pp.151–160.

Taktak, M., Majdoub, M.A., Bentahar, M. and Haddar, M. (2013) 'Numerical characterization of an axisymmetric lined duct with flow using multimodal scattering matrix', *Journal of Theoretical and Applied Mechanics*, Vol. 51, No. 2, pp.313–25.

Taktak, M., Ville, J.M., Haddar, M., Gabard, G. and Foucart, F. (2010) 'An indirect method for the characterization of locally reacting liners', *Journal of the Acoustical Society of America*, Vol. 127, No. 6, pp.3548–3559.

Xu, M. and Cheuk-Ming, M. (2012) 'Wave propagation in a duct with a periodic Helmholtz resonators array', *Journal of the Acoustical of America*, Vol. 131, No. 2, pp.1172.